Automatic DGD and GVD compensation at 640 Gb/s based on scalar radio-frequency spectrum measurement

Paquot, Yvan; Schröder, Jochen; Palushani, Evarist; Neo, Richard; Oxenløwe, Leif Katsuo; Madden, Steve; Choi, Duk-Yong; Luther-Davies, Barry; Pelusi, Mark D.; Eggleton, Benjamin J.

Published in:
Applied Optics

Link to article, DOI:
10.1364/AO.52.001919

Publication date:
2013

Document Version
Publisher's PDF, also known as Version of record

Automatic DGD and GVD compensation at 640 Gb/s based on scalar radio-frequency spectrum measurement

Yvan Paquot,[1,*] Jochen Schröder,[1] Evarist Palushani,[2] Richard Neo,[1] Leif K. Oxenløwe,[2] Steve Madden,[3] Duk-Yong Choi,[3] Barry Luther-Davies,[3] Mark D. Pelusi,[1] and Benjamin J. Eggleton[1]

[1]Centre for Ultrahigh bandwidth Devices for Optical Systems (CUDOS), Institute of Photonics and Optical Science (IPOS), School of Physics A28, University of Sydney, New South Wales 2006, Australia

[2]DTU Fotonik, Technical University of Denmark, Lyngby 2800 Kgs., Denmark

[3]CUDOS, Laser Physics Centre, Australian National University, Canberra ACT 0200, Australia

*Corresponding author: yvan@physics.usyd.edu.au

Received 27 November 2012; revised 7 February 2013; accepted 15 February 2013; posted 15 February 2013 (Doc. ID 180645); published 14 March 2013

We demonstrate what we believe to be the first real-time impairment-cancellation system for group-velocity dispersion (GVD) and differential group delay (DGD) for a 640 Gb/s single-channel signal. Simultaneous compensation of two independent parameters is demonstrated by feedback control of separate GVD and DGD compensators using an impairment monitor based on an integrated all-optical radio-frequency (RF) spectrum analyzer. We show that low-bandwidth measurement of only a single tone in the RF spectrum is sufficient for automatic compensation for multiple degrees of freedom using a multivariate optimization scheme. © 2013 Optical Society of America

OCIS codes: 060.2330, 060.4256.

1. Introduction

The current race to increase bandwidth has led to the development of higher communications data rates on an optical fiber [1]. This includes architectures based on dense wavelength-division multiplexing [2] and optical frequency-division multiplexing [3], the use of advanced modulation formats, such as differential quadrature phase-shift keying and quadrature amplitude modulation [4], and increasing the symbol rate (baud rate) using optical time-division multiplexing (OTDM) [5,6], or combinations of such schemes. All these techniques introduce strong constraints on the transmitters, receivers, and transmission links. In particular, transmission over long distances tends to degrade ultradense signals as a result of both nonlinear (self- and cross-phase modulation, four-wave mixing, Raman) and linear [dispersion, polarization mode dispersion (PMD)] effects [1,7], as well as optical SNR degradation due to amplified spontaneous emission (ASE) occurring in the amplifiers.

Here we investigate the practicality of serial data transmission based on OTDM, recognizing that future systems will exploit a combination of wavelength-division multiplexing, coherent formats, and ultrafast-baud-rate techniques. In the case of OTDM, the bandwidth that can be transmitted in real-world systems reaches a limit due to the sensitivity of ultrashort pulses to multiple sources of degradation along the fiber link. These include group-velocity dispersion (GVD), higher order dispersion [8], and PMD [9].

1559-128X/13/091919-09$15.00/0

Compensation schemes for multiple orders of dispersion are well known and include the use of phase modulators [8], tunable fiber Bragg gratings [10–12], and concatenation of spans of specialty fibers [13,14]. However, fluctuations of the impairments, mainly due to temperature drifts and stress variations, also occur in long-distance fiber transmission, requiring adaptative solutions able to tune the compensation in real time [15–17]. This involves measurement of the impairments and automatic feedback to a tunable compensator. This approach has led to demonstration of automatic PMD compensation [9,18] and, more recently, of automatic simultaneous compensation for GVD and higher orders of dispersion [19].

It is of note that in the context of coherent transmission formats, another common dispersion and differential group delay (DGD) compensation technique uses postprocessing of the received signal in the electrical domain by digital signal processing (DSP) [20,21]. This method has gained substantial interest recently; however, the statement that DSP can mitigate DGD and chromatic-dispersion impairments is not straightforward in the context of OTDM signals. These signals must be demultiplexed to a lower bit rate before they can be converted into an electrical signal. Demultiplexing using sampling techniques [5,6] would require extracting all of the OTDM channels to allow for DSP compensation of the signal. This would remove the ability to extract only one channel at a time out of the OTDM signal. Inserting an optical distortion compensator before the demultiplexer allows for clean detection of one OTDM channel without having to demultiplex all the channels in parallel.

In this paper, we extend our previous work by showing that the automatic feedback method can be applied to simultaneously control multiple compensators and mitigate impairments of different natures. We demonstrate a system for canceling the combined effect of first-order PMD (usually called DGD) and GVD for a 640 Gb/s single-channel OTDM signal.

As in [19], the scheme relies on optical performance monitoring, which is a key function required for automatic impairment mitigation. Ultrahigh–bit-rate OTDM signals can be monitored using techniques based on autocorrelators [22], optical sampling oscilloscopes [23], all-optical 2R (reamplification and reshaping) regenerators [24], measurements of spectral broadening [25], interferometry inside a wavelength-selective switch [26], or all-optical radio-frequency (RF) spectrum analysis [27].

The latter is used in this work to determine the quality of the signal by measuring a single tone in its RF spectrum and does not require determination of the specific values of the parameters being compensated. The single signal-quality monitor drives both GVD and DGD compensators by means of a multivariate optimization algorithm. Our experimental setup uses a spectral pulse shaper (SPS) to compensate dispersion [28], a DGD compensator to split and delay the polarization components [29], and an all-optical RF spectrum analyzer as the ultrahigh-bandwidth signal monitor.

2. Background and Principle

Figure 1 summarizes the strategy used for automatic compensation of DGD and GVD. The signal quality is monitored with an all-optical RF spectrum analyzer with terahertz bandwidth based on a chalcogenide waveguide chip [27]. Only the 640 GHz component of the RF spectrum is monitored, and this is extracted using a bandpass filter (BPF). A decrease in the signal quality corresponds to a reduction in the power of the 640 GHz tone that activates the compensation procedure. The information provided by measurement of this single parameter of the RF spectrum is sufficient to control the 2 degrees of freedom (GVD and DGD) thanks to the use of a hill-climbing algorithm. The fixed-step Powell method [30] was chosen for its simplicity and robustness to noise in the measurement. It was used with the DGD and GVD parameters set as conjugate directions for the optimization.

The absolute optimum configuration can be approached only from within a window with a width of about 1 pulse period on either side of the optimum, because the 640 GHz tone power changes monotonically as a function of both impairments only within that window. This does not mean, however, that the largest DGD or GVD errors that can be corrected are limited, but merely that tracking must start within

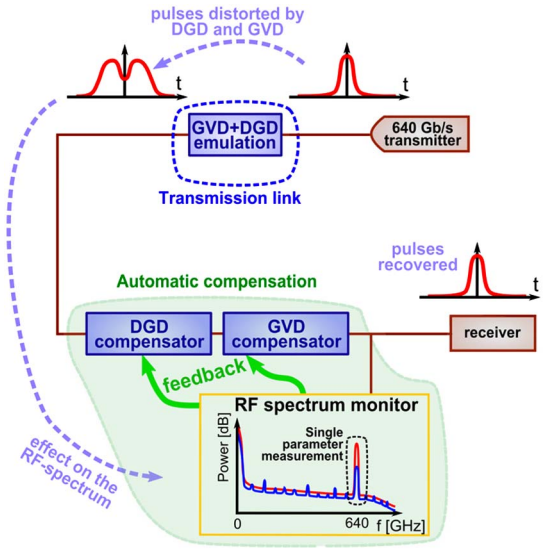

Fig. 1. (Color online) Summary of the compensation strategy. The transmitter is followed by a link emulating both the initial bias and the temporal drifts in GVD and DGD. The automatic compensation system is inserted before the receiver to cancel those impairments using the signal received from the all-optical RF spectrum analyzer (the signal monitor). The figure illustrates how the link distorts the data pulses and this is detected by the signal monitor, which activates the DGD and GVD compensators. GVD causes pulse broadening and DGD pulse splitting, and these both impair the RF spectrum by decreasing the 640 GHz tone (lower trace, bottom).

that window for the compensation to remain accurate. Hence, within this window, increasing the absolute value of either DGD or GVD by a small amount leads to a drop in the tone power. The optimum combination of GVD and DGD introduced by the compensators can thus be found by tuning them successively to maximize the tone power. By running the monitor continuously, the whole transmission link remains locked to the optimum despite any fluctuations of DGD and GVD on the link.

Simultaneous optimization of multiple parameters is allowed by running a multivariate optimization algorithm based on a single "quality factor" parameter (the tone power). The principle of this trial-and-error algorithm is illustrated in Fig. 2. It first selects DGD as the active parameter, keeping the GVD fixed. The value of DGD is changed by small steps in a random direction. If the tone power improves, a further change is made in the same direction; otherwise, the direction is inverted. After four recursive steps, the same process is applied to GVD. If the tone power has not fully recovered to the optimum value, the scheme is repeated until complete compensation of the impairments is achieved.

3. Experiment

Figure 3 shows the whole compensation system. It comprises a transmitter generating the 640 Gb/s OTDM signal encoded with pseudorandom bit sequence (PRBS) data. The optical signal was transmitted through a link made of a dispersion emulator, a DGD emulator, a short fiber section [50 m single-mode fiber (SMF) and 10 m dispersion-compensating fiber (DCF)] and an erbium-doped fiber amplifier. The dispersion and DGD emulators were both tunable devices capable of adding a specific level of impairment at any time during the experiment. The automatic compensation system was inserted after the link in order to recover the signal before the receiver. It is essential that DGD and GVD are exactly compensated to obtain transform-limited data pulses so as to minimize adjacent-channel overlap during the demultiplexing process in the OTDM receiver.

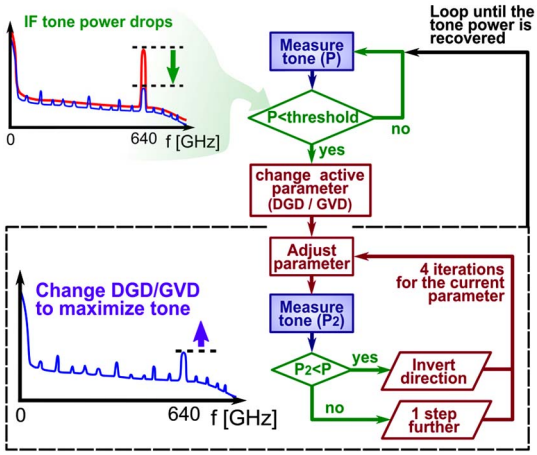

Fig. 2. (Color online) Flow diagram of the optimization algorithm. Detection of a drop in the tone power activates the optimization process. DGD and GVD are successively considered in a loop modifying the active parameter step by step so as to maximize the tone power.

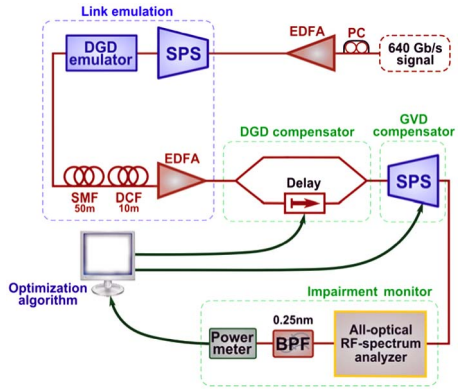

Fig. 3. (Color online) Main building blocks of the compensation experiment: successively, a 640 Gb/s OTDM transmitter, a link emulating DGD and GVD fluctuations with a DGD emulator and an SPS, a DGD compensator, a GVD compensator (SPS), and an RF spectrum analyzer used as broad-bandwidth signal monitor. Feedback from the monitor to the compensators enables automatic compensation.

A. Signal Generation

The experimental test bed used a 640 Gb/s single-channel PRBS data stream constructed by time-interleaving 16 channels of 40 Gb/s bit rate. The 40 Gb/s channels were produced using a mode-locked laser delivering a pulse train at 40 GHz with a pulse width of 1.4 ps. These pulses were then passed through two compression stages to shorten them to 500 fs using spectral broadening in a highly nonlinear fiber and bandpass filtering [31]. The pulse train was then encoded with $2^{31} - 1$ PRBS data using a Mach–Zehnder modulator to create a single data channel at 40 Gb/s. That channel was then replicated and delayed 16 times with interferometric multiplexing stages with a delay of $2^7 - 1$ bit periods in order to form the OTDM channel at 640 Gb/s. The details of the transmitter are shown in Fig. 4.

B. Signal Monitoring

Measurement of the RF spectrum is a common technique for monitoring telecommunications signals. Electronic RF spectrum analyzers are used for bandwidths typically up to 50 GHz [32]. However, these cannot be used for ultrahigh-baud-rate signals, which are far beyond the bandwidth of state-of-the-art electronics. In order to overcome this limitation, we made use of an all-optical equivalent of an RF spectrum analyzer based on nonlinear optics, illustrated in Fig. 5 [27]. Copropagation of the signal under test with a cw probe at another wavelength in a nonlinear medium induces spectral broadening on the probe due to cross-phase modulation. The phase of the probe is modulated in proportion to the instantaneous intensity of the signal. Hence, the

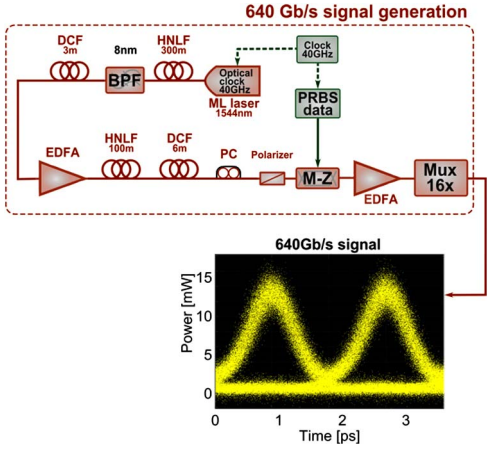

Fig. 4. (Color online) Details of the transmitter. The pulse train from a mode-locked laser is compressed with two nonlinear compression stages, encoded with a Mach–Zehnder modulator driven by PRBS data, and time-interleaved 16 times using interferometric multiplexing stages. The mode-locked laser and the PRBS data generator were synchronized to a unique electronic clock. The lower panel shows an eye diagram of the signal obtained using an optical sampling oscilloscope.

optical spectrum of the probe reflects the Fourier transform of the square of the optical field of the signal, which corresponds to the power spectrum of its intensity, also called the RF spectrum.

In these experiments, the nonlinear medium was a 6.5 cm long As_2S_3 chalcogenide waveguide, which provides the potential for an integrated solution for signal monitoring [33]. The RF spectrum of an optimized signal exhibits a strong DC component (the initial cw probe), background power over the whole spectrum, and tones at the carrier frequency and its multiples. Distortion of the signal induces the appearance of tones at submultiple frequencies and a dramatic drop of the carrier tone power at 640 GHz [34]. A single measurement of the 640 GHz tone is enough to define the quality of the signal in a state close to the optimum. This is based on data such as shown in Fig. 6 and on the previous analysis of the locally monotonic dependence of tone power on dispersion impairment demonstrated in [19]. Interestingly, there is no need to measure the complete RF spectrum for this monitoring method. A simple

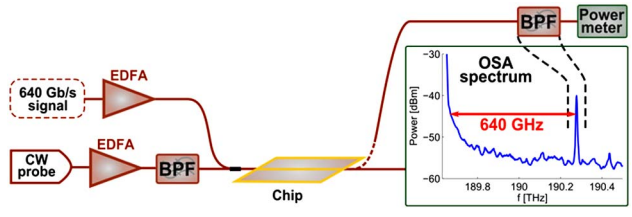

Fig. 5. (Color online) RF spectrum of the signal as measured with terahertz bandwidth by copropagating it with a cw probe at a different wavelength inside a highly nonlinear chalcogenide waveguide. Cross-phase modulation causes spectral broadening in the probe, which reflects the RF spectrum of the signal. The tone power of the spectrum corresponding to the carrier frequency was extracted with a BPF.

narrow-optical BPF with 30 GHz bandwidth centered on the 640 GHz tone placed at the output of the RF spectrum analyzer allows the tone power to be monitored on a slow photodetector. Hence, information on the tone power can be extracted without using an optical spectrum analyzer (OSA).

Despite the fact that the compensators have large working ranges, as discussed below, the signal monitor has a monotonic behavior (i.e., the algorithm can be run deterministically) only over a much smaller range, of the order of the data pulse width. This means that the reading of the signal quality remains valid only for residual dispersion and DGD values within a limited window (typically 1 ps for DGD and 0.15 ps/nm for GVD) centered on the state of a perfectly compensated link. For DGD/GVD mismatch exceeding that window, the algorithm diverges as shown on 10. Thus, the initial state of the compensation system must be set so as to cancel the effect of the link. Once the algorithm is locked, the drift of the parameters can cover the whole range allowed by the DGD and GVD compensation devices as long as the changes are slow enough for the algorithm to track the optimum.

C. DGD Compensator

DGD is defined as the delay between the two principal polarization components caused by the difference in travel time of an optical wave in a birefringent medium [35]. This effect can also be emulated by separating the principal polarization components, delaying one with respect to the other and recombining them [29].

The setup used as a DGD compensator is shown in Fig. 7. The signal was split into two orthogonal polarizations by a polarizing beam splitter (PBS). The polarization state of its input was set at 45° with respect to the principal axes of the PBS in order to match the polarization state arbitrarily set to 45° at the input of the DGD emulator inside the transmission link. This choice is artificial and would be subject to fluctuations in a real transmission application.

Further development of our method could include addition of a computer-controlled polarization controller at the input of the DGD compensator, regulated as two additional degrees of freedom by the same optimization algorithm as used for driving our actual DGD and GVD compensators. Adding a polarization controller in the DGD compensator has proved to improve the performance of the compensation scheme [36]. For higher order PMD control, the wavelength dependence of the DGD should be included [35].

A relative delay was applied between both arms with a computer-controlled programmable delay line (General Photonics MDL-002). This device allows a resolution of 1 fs, which was more than enough to accurately delay the 500 fs duration pulses. A second PBS recombined the two polarizations to form the output beam. Polarization controllers were inserted

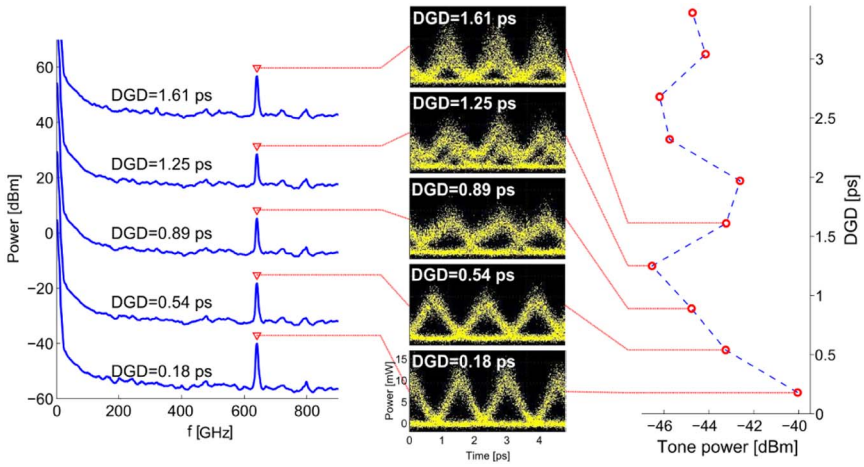

Fig. 6. (Color online) Evolution of the carrier tone power as a function of DGD (left and right panels), suggesting the choice of that parameter as signal-quality indicator. Indeed, an increase of the DGD impairment (as visualized on the series of eye diagrams) causes a drop of the tone power within a range of more than 1 ps around the zero DGD state. The RF spectra presented on the left are shifted upward by multiples of 20 dB for ease of viewing. The actual spectra have an absolute power aligned with the lower graph.

into both arms in order to adjust the polarizations to match the transmitted states of the second PBS. For zero DGD, the delay on both arms must be identical.

Initial setting of the programmable delay line was found by canceling the interference fringes at the output of the DGD compensator, fed with polarized ASE noise, set with a polarization state at 45° with respect to the principal axes. A polarizer at 45° was placed at the output of the compensator to force the two output polarization states into the same plane to generate interference fringes, followed by an OSA. Fringes were observed on the spectrum with a period inversely proportional to the detuning of the delay between both arms. Zero relative delay was found by setting the delay line so as to cancel the fringes.

A commercial device (General Photonics DynaDelay 40G) was used as the DGD emulator. Its working principle is different from the compensator, but it has a similar effect on the signal. However, the same device could not be used as compensator because of its limited resolution of 360 fs, which is too coarse compared with the pulse width of 500 fs and would make the compensation system inaccurate and unstable.

Limitations of the DGD compensator.—The polarization dependence of the impairment monitor (the signal must have the same polarization state as the probe) introduces constraints on the DGD compensator. The interferometric nature of the DGD compensator induces a phase-dependent polarization offset, which would lead to a random polarization at the output of the device if no further care were taken. Phase-periodic choice of the delay in the compensator ensured that the relative phase between both arms was constant. Hence, the polarization state at the input of the RF spectrum analyzer was not affected by the action of the DGD compensator, enabling consistent measurement of the impairment. The change of the DGD state was achieved in two stages. First, the delay was tuned to the rough value of the DGD wanted (with 0.1 ps resolution). Then the delay was stepped with 1 fs resolution over 1 period of the optical wave (about 5.2 fs for a signal at 1558 nm). During the second stage, the power of the 640 GHz tone of the RF spectrum was recorded. The highest power detected determined the signal quality for that value of DGD. For this reason, each optimization step during the experiment took about 10 s.

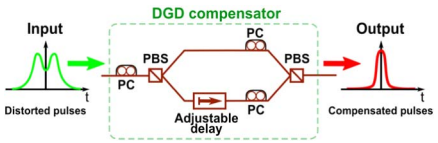

Fig. 7. (Color online) Use of PBSs to split and recombine the two orthogonal polarization states. One arm was directed straight to the second PBS by a length of SMF, and the length of the other was controlled with a programmable delay line. The degradation of the RF spectrum related to a change of DGD by the emulator was recovered by applying an opposite DGD value using the compensator.

Although the fine step of the delay greatly influences the RF spectral measurements, the quality of the eye diagram of the signal does not change significantly as long as the device used to measure it is not polarization dependent. This was verified by monitoring the eye diagram with an optical sampling oscilloscope as the fine delay was changed. The optimization process could be dramatically sped up if a device similar to the one used as the DGD emulator, but with better resolution, could be used as compensator, since the General Photonics DynaDelay 40G is programmed to adjust the delay with consistent phase periodicity.

Some additional noise appeared in our measurements as a result of the limited resolution of the delay line, which could not reliably capture the maximum of the interference peak during the fine sweep.

D. Dispersion Compensator

GVD can be emulated by applying a parabolic spectral phase on the signal. It has been shown that such a spectral phase can be generated using an SPS [37] and that this technique can also emulate higher orders of dispersion. This method was used in [38] for its tunability, broadband action, and ability to emulate multiple orders of dispersion. In this experiment, we used an SPS as GVD compensator for the same reasons.

The SPS used in our experiment allows for a tuning range of ±30 ps/nm [28]. Once locked onto the optimum state canceling residual dispersion, our compensation algorithm can track the optimum over the whole range of the SPS. For initial offsets higher than ±30 ps/nm, dispersion can be roughly compensated by adding DCF to the link. The dispersion slope mismatch between DCF and SMF translates into residual higher orders of dispersion that can be compensated (statically or automatically in the case of strong fluctuations) using our SPS based multi-order dispersion compensator, as shown in [19]. A similar device is also used for dispersion emulation in the transmission link.

4. Results

In this section, we present demonstrations of DGD-only and simultaneous DGD and GVD compensation. The first case demonstrates the stability of the method over a large span of DGD exceeding the duty cycle of the signal, while the second demonstrates that the concept can be extended to the conjugate effect of DGD and GVD, by controlling two separate compensation devices.

In Figs. 8 and 9, the bottom graphs show histograms of the 640 GHz tone power measured after each step. The tone power is the only information that the system has about the impairment level. In that sense, it reflects the quality of the signal

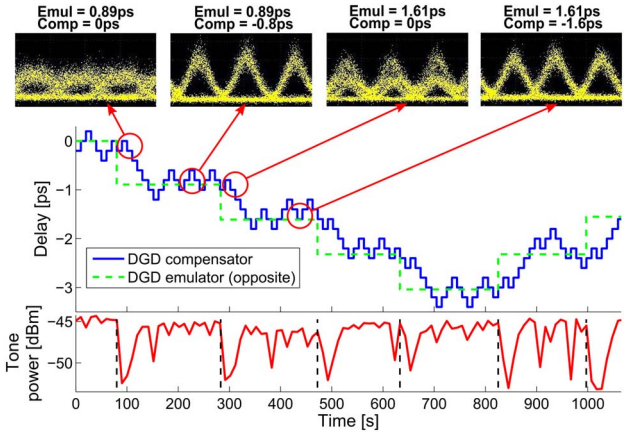

Fig. 8. (Color online) Middle: histogram of the DGD emulated by the link (dashed line) and the DGD applied by the compensator in the opposite direction (solid line). Bottom: histogram of the tone power. The vertical dashed lines show where the DGD changes have been applied. Top: a series of eye diagrams confirming the compensation of the DGD impairment on the signal.

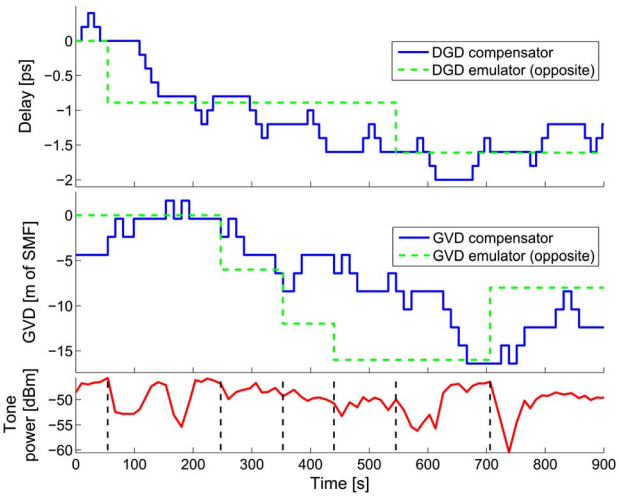

Fig. 9. (Color online) Top: histogram of the DGD emulated by the link (dashed line) and the DGD applied by the compensator in the opposite direction (solid line). Middle: histogram of the GVD emulated by the link (dashed line) and the GVD applied by the compensator in the opposite direction (solid line). Bottom: histogram of the tone power. The vertical dashed lines show where the DGD and GVD changes have been applied.

at the output of the compensator. However, this statement has to be understood carefully given the limitations discussed in Section 3 about the DGD compensator. Indeed, the strong fluctuations appearing occasionally on the RF tone-power histogram (e.g., at 150 s in Fig. 9) are due to errors in the measurement and do not imply that the signal itself was impaired. These random measurement errors arise from the fact that our homemade DGD compensator does not accurately step through the delay by an integer number of carrier cycles, leading to interference issues between the two polarization components when forced into the same plane (the RF spectrum analyzer acts like a polarizer when measuring the signal). However, these fluctuations do not affect the signal measured by an intensity detector for bit error rate testing. Commercial devices such as the one we used as DGD emulator (General Photonics DynaDelay 40G) are calibrated so as to avoid that problem, so that the issue would not appear in a real-world solution. The step size used in the algorithm is chosen small enough so as to be robust to punctual errors in the signal measurement—moving by one step in the wrong direction does not significantly affect the eye diagram.

The upper graphs record the evolution of the DGD in the case of Fig. 8 (middle), and both DGD and GVD in Fig. 9 (middle, top) with the opposite of the values introduced by the emulator(s) shown by dashed lines and the compensator(s) by solid lines. The compensators need to introduce values of DGD and GVD that are opposite to the emulators' in order to cancel their effects.

As demonstrated in Fig. 8, after an initial settling time of about 50 s, the DGD states of the compensator successfully tracked that of the emulator. The eye diagrams shown at the top of Fig. 8 demonstrate that

the compensation system was working properly, with open "eyes" being recovered after the changes in the emulator settings. In Fig. 8, the reaction of the system to a degradation of the signal is reasonably rapid, and the DGD applied by the compensator immediately moves in the correct direction. The compensation trace appears as a piecewise stair function as a result of the fact that the optimization algorithm proceeds by trial and error with a fixed step size.

An increase in the number of degrees of freedom to be successively optimized by the hill-climbing algorithm results in a slower overall response of the system. In the case of multiple-parameter optimization, shown in Fig. 9, the compensators take longer to stabilize to the correct values because of the increased complexity of the optimization process. This appears clearly in Fig. 9, where the states of the DGD and GVD compensators do not immediately follow the emulators and sometimes oscillate before converging. In order to push the system to its limits, random state changes were applied between times of 250 and 600 s without waiting for complete stabilization of the system after each change. As a consequence, the tone power did not have the time to recover its optimum value and the compensators did not match the emulators during this transient period. However, when letting the system recover after the time 550 s, the compensation device successfully brought the tone power back to its highest value and the states of the compensators got close to the emulators.

5. Discussion

The experimental results presented in Section 4 involve abrupt changes in emulated DGD and GVD, while in a real-world application, the fluctuations are more likely to be smooth drifts, for example, due to slow temperature fluctuations, which are easier to track for an optimization algorithm. Thus our experiments present a worst-case scenario.

Comparison of our system with real DGD and GVD drifts data allows one to evaluate the range of applications of the device. Data on temperature dependence of DGD can be found in [39]. The worst case of DGD oscillations during this experiment (36 km fibre, temperature increase by 30°C over 250 min) was about 0.00042 ps/km/min. Our system allows for a compensation rate around 0.5 ps/min, which is more than enough for links of a few tens of kilometers. Data for GVD can be found in [17]. The worst fiber studied presented a temperature dependence of −0.003 ps/nm/km/K. Our system allows for a compensation rate around 0.08 ps/nm/min, which is enough to stabilize a link of 10 km subject to a temperature change of 10°C over 1 h.

The settling times considered here correspond to sharp changes in dispersion and DGD, which is a worst-case approach. Real-world fluctuations due to temperature changes would more likely see smooth drifts of the parameters. Also, the whole process could in principle be sped by up to a factor of 100. Indeed, the use of a correctly calibrated DGD compensator would avoid the 10 s/step measurement time due to fine tuning of the delay. Use of faster control interfaces between the decision logic and the SPS and power meter would also reduce the time of a single cycle of the algorithm.

Figure 10 compares the DGD-compensated transmission link affected by a sharp DGD change for three cases. If the compensation feedback is inactive (left), the signal is permanently degraded by the DGD change. When the DGD compensation system is used within its working range (middle), DGD fluctuations are canceled and the signal recovers. If the compensator is active but the fluctuations applied to the link are greater than the permissible range (see Fig. 6, right; the tone power rises with a period equal to the period of the signal), the optimization process is likely to diverge to a local maximum, leading to a permanent DGD mismatch. Hence the signal cannot be recovered. Similar behavior is observed for the GVD compensation.

Decreasing the noise from the RF spectrum monitor would allow a reduction in the step size set in the optimization algorithm, smoothing the "stairs" in the evolution of the compensator states and improving the stability of the compensated signal. As discussed in Section 3, the DGD compensator is a major source of noise due to inaccurate phase control, leading to polarization fluctuations that affect the measurement of the RF spectrum. Replacing the homemade DGD compensator by a device similar to the emulator, but with better resolution, would improve the results a great deal by avoiding the issue of phase sensitivity of the DGD value applied.

In the future, automatic higher order PMD compensation could be implemented based on the same

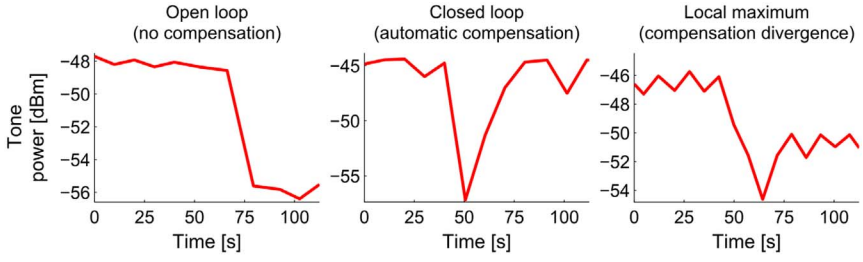

Fig. 10. (Color online) Histograms of the tone power while monitoring a system subject to sharp DGD changes. Left: the automatic DGD compensation system is turned off; the degraded signal is not recovered. Middle: the automatic DGD compensation system is turned on; the tone power quickly recovers its maximum value. Right: the DGD compensation system is on, but the DGD change applied is too high to allow for stable compensation; the system is pushed to a local maximum.

technique, by considering each PMD order as additional degrees of freedom in the optimization process. The DGD compensator should then be updated to allow compensation for higher order PMD. Addition of a computer-controlled polarization controller at the input of the existing DGD compensator would allow for first- and second-order PMD control [29,36].

Finally, it should be noted that a drop in the tone power caused by possible changes in the coupling ratio of the chip, amplifier failure, or any other nondispersive impairment would not necessarily prevent the operation of this automatic dispersion compensator, which seeks to relocate a global maximum in tone power, whatever the absolute power level is.

6. Conclusion

Our results consolidate our RF spectrum analyzer as a multipurpose impairment monitor for ultrahigh-symbol-rate signals. We have demonstrated that the multivariate optimization method based on the single measurement of the carrier tone power can be used for simultaneous compensation of impairments of different natures. Application of the method to the control of GVD and DGD compensators provided the first successful demonstration, to our knowledge, of automatic simultaneous DGD and GVD compensation for ultrahigh-symbol-rate transmission.

The authors acknowledge the Australian Research Council (ARC) Centres of Excellence Program (Project CE110001018), Federation Fellowship (Project FF0776056), Future Fellowship (Project FT110100853), and Discovery Early Career Researcher Award (DECRA) (Project DE120101329) and an ARC Linkage Grant with Finisar Australia (Project LP120100661).

References

1. I. P. Kaminow, T. Li, and A. E. Willner, eds., *Optical Fiber Telecommunications V, A: Components and Subsystems*, 5th ed. (Academic, 2008).
2. A. H. Gnauck, G. Charlet, P. Tran, P. J. Winzer, C. R. Doerr, J. C. Centanni, E. C. Burrows, T. Kawanishi, T. Sakamoto, and K. Higuma, "25.6 Tb/s WDM transmission of polarization-multiplexed RZ-DQPSK signals," J. Lightwave Technol. **26**, 79–84 (2008).
3. D. Qian, M.-F. Huang, E. Ip, Y.-K. Huang, Y. Shao, J. Hu, and T. Wang, "101.7 Tb/s (370 × 294 Gb/s) PDM-128QAM-OFDM transmission over 3 × 55 km SSMF using pilot-based phase noise mitigation" in *National Fiber Optic Engineers Conference*, OSA Technical Digest (CD) (Optical Society of America, 2011), paper PDPB5.
4. P. J. Winzer and R.-J. Essiambre, "Advanced modulation formats for high-capacity optical transport networks," J. Lightwave Technol. **24**, 4711–4728 (2006).
5. M. Nakazawa, E. Yoshida, T. Yamamoto, E. Yamada, and A. Sahara, "TDM single channel 640 Gbit/s transmission experiment over 60 km using 400 fs pulse train and walk-off free, dispersion flattened nonlinear optical loop mirror," Electron. Lett. **34**, 907–908 (1998).
6. T. Richter, E. Palushani, C. Schmidt-Langhorst, M. Nölle, R. Ludwig, and C. Schubert, "Single wavelength channel 10.2 Tb/s TDM-data capacity using 16-QAM and coherent detection," in *National Fiber Optic Engineers Conference*, OSA Technical Digest (CD) (Optical Society of America, 2011), paper PDPA9.
7. G. P. Agrawal, *Nonlinear Fiber Optics*, 3rd ed. (Academic, 2001).
8. M. Nakazawa, T. Yamamoto, and K. R. Tamura, "1.28 Tbits/s – 70 km OTDM transmission using third- and fourth-order simultaneous dispersion compensation with a phase modulator," Electron. Lett. **36**, 2027–2029 (2000).
9. H. Sunnerud, M. Westlund, J. Li, J. Hansryd, M. Karlsson, P.-O. Hedekvist, and P. Andrekson, "Long-term 160 Gb/s-TDM, RZ transmission with automatic PMD compensation and system monitoring using an optical sampling system," in *ECOC '01: 27th European Conference on Optical Communication* (IEEE, 2001), Vol. **6**, pp. 18–19.
10. B. Eggleton, B. Mikkelsen, G. Raybon, A. Ahuja, J. A. Rogers, P. S. Westbrook, T. N. Nielsen, S. Stulz, and K. Dreyer, "Tunable dispersion compensation in a 160 Gb/s TDM system by a voltage controlled chirped fiber Bragg grating," IEEE Photon. Technol. Lett. **12**, 1022–1024 (2000).
11. S. Wielandy, P. S. Westbrook, M. Fishteyn, P. Reyes, W. Schairer, H. Rohde, and G. Lehmann, "Demonstration of automatic dispersion control for 160 Gbits/s transmission over 275 km of deployed fibre," Electron. Lett. **40**, 690–691 (2004).
12. M. Durkin, M. Ibsen, M. Cole, and R. Laming, "1 m long continuously-written fibre Bragg gratings for combined second- and third-order dispersion compensation," Electron. Lett. **33**, 1891–1893 (1997).
13. C. D. Poole, J. M. Wiesenfeld, D. J. DiGiovanni, and A. M. Vengsarkar, "Optical fiber-based dispersion compensation using higher order modes near cutoff," J. Lightwave Technol. **12**, 1746–1758 (1994).
14. A. Sano, T. Kataoka, M. Tomizawa, K. Hagimoto, K. Sato, K. Wakita, and K. Kato, "Automatic dispersion equalization by monitoring extracted-clock power level in a 40 Gbit/s, 200 km transmission line," in *ECOC '96: 22nd European Conference on Optical Communication* (IEEE, 1996), Vol. **2**, pp. 207–210.
15. F. Heismann, D. A. Fishman, and D. L. Wilson, "Automatic compensation of first-order polarization mode dispersion in a 10 Gb/s transmission system," in *24th European Conference on Optical Communication* (IEEE, 1998), Vol. **1**, pp. 529–530.
16. M. Karlsson, J. Brentel, and P. A. Andrekson, "Long-term measurement of PMD and polarization drift in installed fibers," J. Lightwave Technol. **18**, 941–951 (2000).
17. M. J. Hamp, J. Wright, M. Hubbard, and B. Brimacombe, "Investigation into the temperature dependence of chromatic dispersion in optical fiber," IEEE Photon. Technol. Lett. **14**, 1524–1526 (2002).
18. T. Takahashi, T. Imai, and M. Aiki, "Automatic compensation technique for timewise fluctuating polarization mode dispersion in in-line amplifier systems," Electron. Lett. **30**, 348–349 (1994).
19. Y. Paquot, J. Schröder, J. Van Erps, T. D. Vo, M. D. Pelusi, S. Madden, B. Luther-Davies, and B. J. Eggleton, "Single parameter optimization for simultaneous automatic compensation of multiple orders of dispersion for a 1.28 Tbaud signal," Opt. Express **19**, 25512–25520 (2011).
20. S. J. Savory, G. Gavioli, R. I. Killey, and P. Bayvel, "Transmission of 42.8 Gbit/s Polarization multiplexed NRZ-QPSK over 6400 km of standard fiber with no optical dispersion compensation," in *OFC/NFOEC 2007: Conference on Optical Fiber Communication and the National Fiber Optic Engineers Conference* (IEEE, 2007), pp. 1–3.
21. F. Buchali and H. Bülow, "Adaptive PMD compensation by electrical and optical techniques," J. Lightwave Technol. **22**, 1116–1126 (2004).
22. J. P. Curtis and J. E. Carroll, "Autocorrelation systems for the measurement of picosecond pulses from injection lasers," Int. J. Electron. **60**, 87–111 (1986).
23. I. Shake, W. Takara, S. Kawanishi, and Y. Yamabayashi, "Optical signal quality monitoring method based on optical sampling," Electron. Lett. **34**, 2152–2154 (1998).
24. P. S. Westbrook, S. Hunsche, G. Raybon, T.-H. Her, and B. J. Eggleton, "Measurement of pulse degradation using all-optical 2R regenerator," Electron. Lett. **38**, 1193–1194 (2002).

25. P. S. Westbrook, B. J. Eggleton, G. Raybon, S. Hunsche, and T.-H. Her, "Measurement of residual chromatic dispersion of a 40 Gb/s RZ signal via spectral broadening," IEEE Photon. Technol. Lett. **14**, 346–348 (2002).
26. J. Schröder, O. Brasier, J. Van Erps, M. A. F. Roelens, S. Frisken, and B. J. Eggleton, "OSNR monitoring of a 1.28 Tbaud signal by interferometry inside a wavelength-selective switch," J. Lightwave Technol. **29**, 1542–1546 (2011).
27. M. Pelusi, F. Luan, T. D. Vo, M. R. E. Lamont, S. J. Madden, D. A. Bulla, D.-Y. Choi, B. Luther-Davies, and B. J. Eggleton, "Photonic-chip-based radio-frequency spectrum analyser with terahertz bandwidth," Nat. Photonics **3**, 139–143 (2009).
28. M. A. F. Roelens, S. Frisken, J. A. Bolger, D. Abakoumov, G. Baxter, S. Poole, and B. J. Eggleton, "Dispersion trimming in a reconfigurable wavelength selective switch," J. Lightwave Technol. **26**, 73–78 (2008).
29. M. Wegmuller, S. Demma, C. Vinegoni, and N. Gisin, "Emulator of first- and second-order polarization-mode dispersion," IEEE Photon. Technol. Lett. **14**, 630–632 (2002).
30. W. H. Press, S. A. Teukolsky, W. T. Vetterling, and B. P. Flannery, *Numerical Recipes: The Art of Scientific Computing*, 3rd ed. (Cambridge University, 2007).
31. T. Inoue and S. Namiki, "Pulse compression techniques using highly nonlinear fibers," Laser Photon. Rev. **2**, 83–99 (2008).
32. Y. K. Lizé, L. Christen, J.-Y. Yang, P. Saghari, S. Nuccio, A. E. Willner, and R. Kashyap, "Independent and simultaneous monitoring of chromatic and polarization-mode dispersion in OOK and DPSK transmission," IEEE Photon. Technol. Lett. **19**, 2006–2008 (2007).
33. D.-Y. Choi, S. Madden, D. A. Bulla, R. Wang, A. Rode, and B. Luther-Davies, "Submicrometer-thick low-loss As_2S_3 planar waveguides for nonlinear optical devices," IEEE Photon. Technol. Lett. **22**, 495–497 (2010).
34. T. D. Vo, M. D. Pelusi, J. Schröder, F. Luan, S. J. Madden, D.-Y. Choi, D. A. P. Bulla, B. Luther-Davies, and B. J. Eggleton, "Simultaneous multi-impairment monitoring of 640 Gb/s signals using photonic chip based RF spectrum analyzer," Opt. Express **18**, 3938–3945 (2010).
35. J. Gordon, "PMD fundamentals: polarization mode dispersion in optical fibers," Proc. Natl. Acad. Sci. USA **97**, 4541–4550 (2000).
36. H. Sunnerud, C. Xie, M. Karlsson, R. Samuelsson, and P. A. Andrekson, "A comparison between different PMD compensation techniques," J. Lightwave Technol. **20**, 368–378 (2002).
37. A. M. Weiner, J. P. Heritage, and E. M. Kirschner, "High-resolution femtosecond pulse shaping," J. Opt. Soc. Am. B **5**, 1563–1572 (1988).
38. J. Van Erps, J. Schröder, T. D. Vo, M. D. Pelusi, S. Madden, D.-Y. Choi, D. A. Bulla, B. Luther-Davies, and B. J. Eggleton, "Automatic dispersion compensation for 1.28 Tb/s OTDM signal transmission using photonic-chip-based dispersion monitoring," Opt. Express **18**, 25415–25421 (2010).
39. J. Cameron, L. Chen, X. Bao, and J. Stears, "Time evolution of polarization mode dispersion in optical fibers," IEEE Photon. Technol. Lett. **10**, 1265–1267 (1998).